Kinetics of Molecular Decomposition under Irradiation of Gold Nanoparticles with Nanosecond Laser Pulses – A 5-Bromouracil Case Study

Telma S. Marques,[#[c,f]] Robin Schürmann,[#[a,b]] Kenny Ebel,[[a,b]] Christian Heck,[[a]] Małgorzata A. Śmiałek,[[c,d]] Sam Eden,[[c]] Nigel Mason,[[c,e]] and Ilko Bald*[[a,b]]

[a] Dr. R. Schürmann, K. Ebel, Prof. Dr. I. Bald
Physical Chemistry, Institute of Chemistry,
University of Potsdam
Karl-Liebknecht-Str. 24-25, 14476 Potsdam-Golm, Germany
E-mail: bald@uni-potsdam.de

[b] Dr. R. Schürmann, K. Ebel, Prof. Dr. I. Bald
Department of Analytical Chemistry
BAM, Federal Institute of Material Research and Testing
Richard-Willstätter-Str. 11, 12489 Berlin, Germany

[c] T. Marques, Dr. S. Eden, Dr. M. A. Śmiałek, Prof N. Mason
Department of Physical Sciences, The Open University, Walton Hall, MK7 6AA, Milton Keynes, UK

[d] Dr. M. A. Śmiałek,
Department of Control and Power Engineering, Faculty of Ocean Engineering and Ship Technology, Gdansk University of Technology, Gabriela Narutowicza 11/12, 80-233 Gdansk, Poland

[e] Prof N. Mason
School of Physical Sciences, University of Kent at Canterbury CT2 7NH, United Kingdom

[f] T. S. Marques
CEFITEC, Departamento de Física, Faculdade de Ciências e Tecnologia, Universidade Nova de Lisboa, 2829-516 Caparica, Portugal

# Authors contributed equally to the manuscript.

* Corresponding author. E-mail: bald@uni-potsdam.de

Abstract:

Laser illuminated gold nanoparticles (AuNPs) efficiently absorb light and heat up the surrounding medium, which enables versatile applications ranging from plasmonic catalysis to cancer photothermal therapy. Therefore, an in depth understanding of the thermal, optical and electron induced reaction pathways is required. Here, the electrophilic DNA nucleobase analogue 5-Bromouracil (BrU) has been used as a model compound to study its decomposition in the vicinity of AuNPs illuminated with intense ns laser pulses under various conditions. The plasmonic response of the AuNPs and the concentration of BrU and resulting photoproducts have been tracked by UV-Vis spectroscopy as a function of the irradiation time. A kinetic model has been developed to determine the reaction rates of two parallel fragmentation pathways of BrU and their dependency on laser fluence and adsorption on the AuNP has been evaluated. In addition, the size and the electric field enhancement of the decomposed AuNPs have been determined by atomic force microscopy (AFM) and finite domain time difference (FDTD) calculations, respectively. A minor influence of direct photoreaction and a strong effect of the heating of the AuNPs has been revealed. However, due to size reduction of the irradiated AuNPs, a trade-off between laser fluence and plasmonic response of the AuNPs has been observed. Hence, the decomposition of the AuNPs might be limiting the achievable temperatures under irradiation with several laser pulses. These findings need to be considered for an efficient design of catalytic plasmonic systems.

Introduction:

Gold nanoparticles (AuNPs) provide versatile applications in the fields of sensing[16,37], catalysis[41] and cancer therapy[1,14]. Localized surface plasmons (LSPs), collective oscillations of the conduction band electrons, are responsible for the outstanding optical properties of AuNPs and can be excited by the alternating electric field of incident light. LSPs strongly enhances the electric field around the nanoparticle, especially when the frequency of the light matches the eigenfrequency of the LSP resonance (LSPR). LSPs can decay in a non-radiative pathway by forming electron-hole pairs, which is typically the initial step in plasmon mediated catalysis[7,27,41]. Since the energy of these plasmonically generated electrons exceeds the thermal equilibrium of the electron gas, they rapidly distribute their energy via electron-electron scattering in the electron gas and subsequently heat up the lattice of the NPs and the surrounding medium[13,21]. Under irradiation with intense ns laser pulses the temperature of the AuNPs can easily be raised to some 1000 K[30], which causes surface evaporation and fragmentation of the AuNPs[11], even under irradiation with a single laser shot.[42] In this process, the morphology of the transformed AuNPs crucially depends on the irradiation parameters.[40] Furthermore, a high temperature and pressure region is generated around the AuNPs, if the laser intensity is sufficiently high.[12] The properties of these nanobubbles are highly dependent on the size of the nanoparticles and the properties of the laser pulse.[17,36] Under illumination of AuNPs with focused laser pulses the generation of reactive secondary species such as singlet oxygen[6] and low energy electrons has been obeserved.[38] As high temperatures are required for the thermionic emission process[20] a threshold for the efficient generation of electrons is expected, which depends on the size of the AuNPs. Biomolecules, like DNA[24,25,32] or proteins[23,31,33], located in a nanoscopic volume around such irradiated AuNPs are efficiently decomposed under laser illumination. In that context, the adsorption of the molecules to the AuNPs surface is strongly influencing the decomposition process, since on the one hand the number of molecules in the high energy in pressure region is increased and on the other hand the aggregation process of the AuNPs determining the size and consequently the plasmonic response is guided by the capping molecules.[25,34] Especially the decomposition of DNA is of particular interest for future applications in cancer photothermal therapy, where cancer cells are killed by an increase of heat mediated by incorporated laser illuminated AuNPs.[1,3] The irradiation of biological tissue with intensive laser pulses leads to an efficient damage, as beyond the Joule-heating versatile nanoscopic effects around the AuNPs are enhancing the cellular damage.[5] Even though the effects occurring in the vicinity of AuNPs illuminated with ns-laser pulses has been widely studied, their action on biomolecules in the surrounding medium on the molecular scale is not yet fully understood. The DNA nucleobase analogue 5-Bromouracil (BrU) was discussed to be a potential DNA radiosensitizer in cancer radiation therapy[19] and consequently its reactions have been extensively studied previously[22,39]. For this purpose, BrU will be used as a model compound to study the reactions in the vicinity of AuNPs under pulsed laser irradiation. Brominated nucleobases are known to be highly reactive towards low energy electrons.[2,22,26,28] The attachment of an electron with a kinetic energy close to 0 eV resonantly cleaves the carbon bromide bond of the nucleobases.[2,28] This reaction has been observed recently on the surface of noble metal NPs triggered by plasmonically generated electrons.[26] However, this electron induced reaction occurs close to the surface of the NPs where the highest temperatures occur and consequently the desorption of the reaction products without further decomposition is very unlikely.

In order to obtain an in-depth understanding of the molecular decomposition processes in the surrounding of laser illuminated AuNPs, the kinetics of different reaction pathways of BrU are studied as a function of irradiation related parameters within the present work. By monitoring the photoproducts of irradiated

BrU as well as optical and morphological properties of the irradiated AuNPs in parallel, the tunability of the plasmon catalyed system can be evaluated.

2. Experimental Details:

2.1 Chemicals:

40 nm AuNPs have been purchased from BBI solutions. BrU has been purchased from Sigma Aldrich and was dissolved in ultrapure water obtained with a Milli-Q water purification system.

2.2 Laser irradiation:

In Figure 1 a scheme of the experimental setup is shown. Ns Laser pulses have been generated using the second harmonic of a Minilite I (Continuum) Nd:YAG laser at 532 nm with an energy of 16 mJ per pulse and a pulse width of 3-5 ns. Until otherwise mentioned a repetition rate of 15 Hz has been used. The laser beam has been widened by a set of two lenses from a diameter of 3 mm to 9 mm. Subsequently the beam has been guided by a dichroic mirror to a further lens (*f = 5 cm*) and focused in a 3.5 ml quartz cuvette (Hellma) slightly above the surface of the AuNP solution. The cuvette is filled with 2 ml of solution, typically containing 45 pM AuNPs and 40 µM BrU, and placed on a stirring plate to stir the solution during the irradiation. Using a mechanical stage, the distance of the laser focus to the surface of the AuNP solution has been varied, to adjust the spot size and in consequence the laser fluence of the divergent beam on the surface. The laser fluences given below refer to the maximum laser fluence at the surface, not considering that the beam is widened as it passes the cuvette. The size of the focused laser beam has been determined using an optical microscope and a blackened photographic paper irradiated with a single laser shot.

2.3 Analytical methods:

UV-Vis extinction spectra were recorded with a Jasco 650 Photospectrometer. Dried AuNPs have been imaged with an Agilent 5500 atomic force microscope (AFM) using a Tap 150 cantilever in the tapping mode. For the sample preparation a 2 µl droplet of the irradiated AuNP solution have been dried on a freshly cleaved mica substrate. The size distribution of the AuNPs on the substrate has been determined from the height of the AuNPs in the AFM images by using the software Gwyddion 2.48.

2.4 FDTD Calculations:

FDTD calculations of the electric field enhancement of AuNPs in an aqueous medium has been carried out with the software Lumerical FDTD Solutions 8.6.3, using a mesh size of 0.1 nm in the plotted areas. The excitation wavelength was set to 532 nm.

3. Results and discussions:

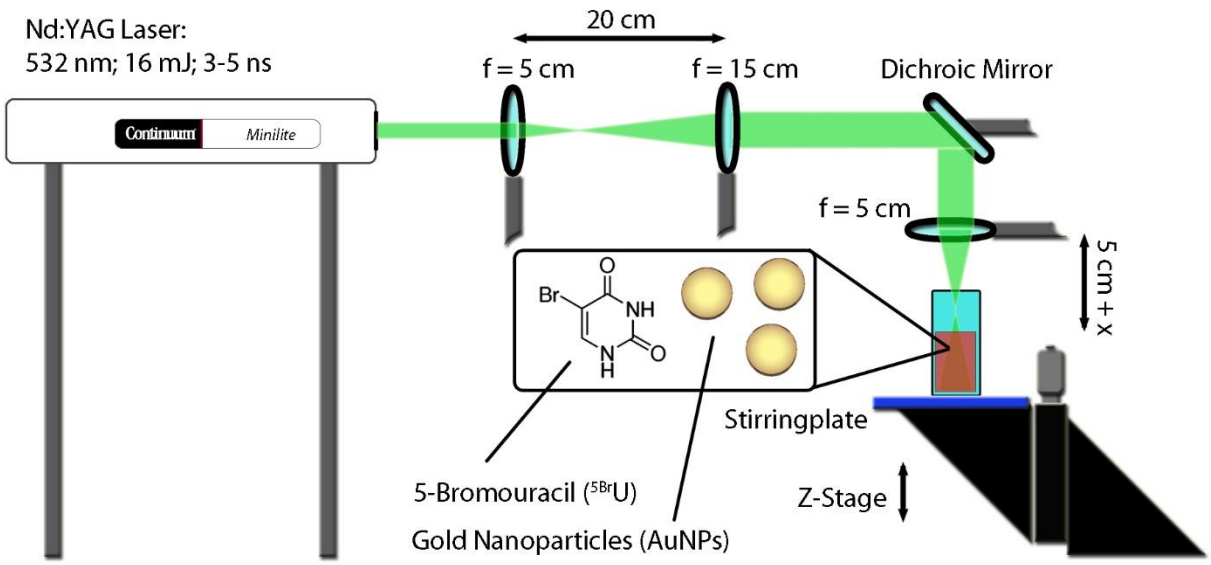

Figure 1: Schematic representation of the experimental setup.

Using the experimental setup presented in Figure 1 a mixture of AuNPs and BrU has been irradiated with ns laser pulses. UV-Vis spectra have been recorded after specific illumination times in order to determine the LSPR of the AuNPs and the π- π* resonance of BrU. In Figure 2 a) a typical dataset is presented showing that the LSPR, which is initially located at 528 nm, is decreased and blue shifted with ongoing irradiation. This change of the LSPR is caused by the decomposition of the AuNPs into smaller fragments. Already after 5 min of irradiation only small changes of the LSPR are observable, which indicates only slight changes in the size distribution and thus approximately constant reaction conditions for the molecular decomposition can be assumed. Moreover, also the intensity of the π- π* transition of the BrU, located at 277 nm[8], is reduced and shifted to lower wavelength during the irradiation. The decrease of the π- π* resonance is attributed to a cleavage of the aromatic ring structure, whereas the shift of the resonance maximum is indicating a chemical modification of the BrU, most likely the cleavage of the C-Br bond leaving the residual molecule intact.[24]

In order to further analyze the π- π* transition, all additional contributions of the solution to the extinction in this wavelength regime need to be determined to correct the background of the BrU spectra (see Figure 2 b)). Therefore, AuNPs have been irradiated in absence of BrU under the same experimental conditions, as the absorption of AuNPs in the UV caused by interband transitions depends significantly on the particle size.

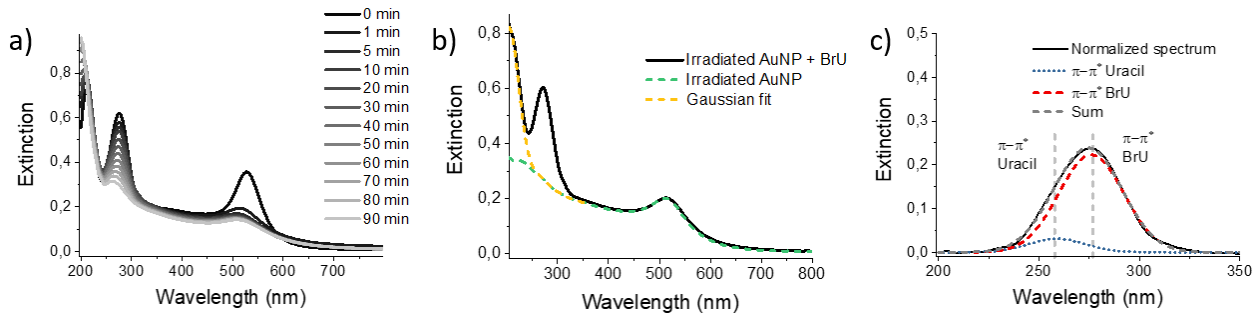

Figure 2: a) UV-Vis spectra of AuNP/BrU solution irradiated with a focused 532 nm ns laser pulses with a repetition rate of 15 Hz with a maximum laser fluence of 3.4 10^{12} W/m^2. b) UV-Vis spectra of irradiated AuNP/BrU solution (black), a spectrum of illuminated AuNPs under the same conditions (green, dashed) and a gaussian fit of the peak centered below 210 nm (yellow, dashed). c) π- π signal (black) corrected by the contributions marked in b). The gaussian fit of the contributions of U (blue) and BrU (red) and their sum (grey) are plotted with dotted lines.*

The spectra of irradiated AuNP solution have been subtracted from the spectra of the irradiated AuNP/BrU solution. In addition, the absorption band located below 210 nm has been fit with a gaussian peak and subtracted from the AuNP/BrU spectra, since there are slight contributions of these signals to the π- π* peak. To determine the contributions of the π- π* transitions of BrU and U, the background corrected AuNP/BrU spectra of the π- π* transition, shown in Figure 2 c), have been fit with two gaussian peaks centered at 277 nm and 258 nm[10], respectively. In this way the concentration *[BrU]* of BrU and *[U]* of U can be monitored as a function of the irradiation time.

In order to explain the shift and the decrease of the π- π* signal two reaction pathways are assumed: the fragmentation of the molecular ring leading to a decrease of the π- π* resonance:

$$BrU \overset{k1}{\rightarrow} small\ fragments \qquad (1)$$

and the cleavage of the C-Br bond resulting in the formation of Uracil (U):

$$BrU \overset{k2}{\rightarrow} U \qquad (2)$$

k_1 and k_2 denote the reaction rates for the fragmentation of the ring and the cleavage of the C-Br bond, respectively. In addition, also a third reaction with a reaction rate k_3 needs to be considered, since the generated U will also be decomposed under laser irradiation in the presence of AuNPs into smaller fragments.

$$U \overset{k3}{\rightarrow} small\ fragments \qquad (3)$$

Based on equation (1) and (2) the decomposition of BrU is following a (pseudo-) first order reaction that can be described by the following equation:

$$\frac{d[BrU]}{dt} = -k_1[BrU] - k_2[BrU] \qquad (4)$$

According to equation (2) and (3) the generation and decomposition of U can be described by:

$$\frac{d[U]}{dt} = -k_3[U] + k_2[BrU] \qquad (5)$$

From equation (4) we get for the concentration of BrU, *[BrU]*, after an irradiation time *t*:

$$[BrU] = [BrU]_0 e^{-(k_1+k_2)t} \qquad (6)$$

Where $[BrU]_0$ is the initial concentration of BrU before the irradiation. Since there has been initially no U in the solution, we set $[U_0] = 0$ and get for [U] (see SI for details):

$$[U] = \frac{k_2[BrU]_0}{k_3-k_1-k_2}\left(e^{-(k_1+k_2)t} - e^{-k_3 t}\right) \quad (7)$$

Consequently, the ratio of [U] and [BrU] can be determined using equation (6) and (7):

$$\frac{[U]}{[BrU]} = \frac{k_2}{k_3-k_1-k_2}\left(1 - e^{-(k_3-k_1-k_2)t}\right) \quad (8)$$

By using the Taylor expansion: $e^x \approx 1 + x$ we can simplify the expression for short illumination times t to:

$$\frac{[U]}{[BrU]} \approx k_2 t \qquad (9)$$

With this equation the reaction rate k_2 can be determined from the ratio of the concentrations *[BrU]* and *[U]*, which can be determined from the intensity of the π-π* resonances at 258 nm and 277 nm in the UV-Vis spectra as a function of the irradiation time *t* (see Figure 3 a)). Error bars have been determined from the background subtraction of the AuNP signal in the absence of BrU and the fits are presented in Fig. 2 b) and c). Due to the strong changes of the AuNP size after the first laser pulses (see text below and Figure 6) influencing the reaction conditions the data points after 0 min and 1 min irradiation time have not been taken into account in the analysis. The determined ratio of *[BrU]* and *[U]* typically follows the expected linear trend after the particle size remains constant.

In Figure 3 b) *[BrU]* is plotted as a function of *t* and fit with an exponential decay, hence, the sum of the reaction rates k_1 and k_2 can be determined from the fit by using equation (6). However, for short and very long irradiations times the exponential correlation is only valid in a first approximation, due to an increased signal to background ratio of the π- π* resonance for long illumination times. Therefore, based on the experimental data it cannot be finally excluded that the reaction might also follow a 0^{th} or some more complex reaction order.

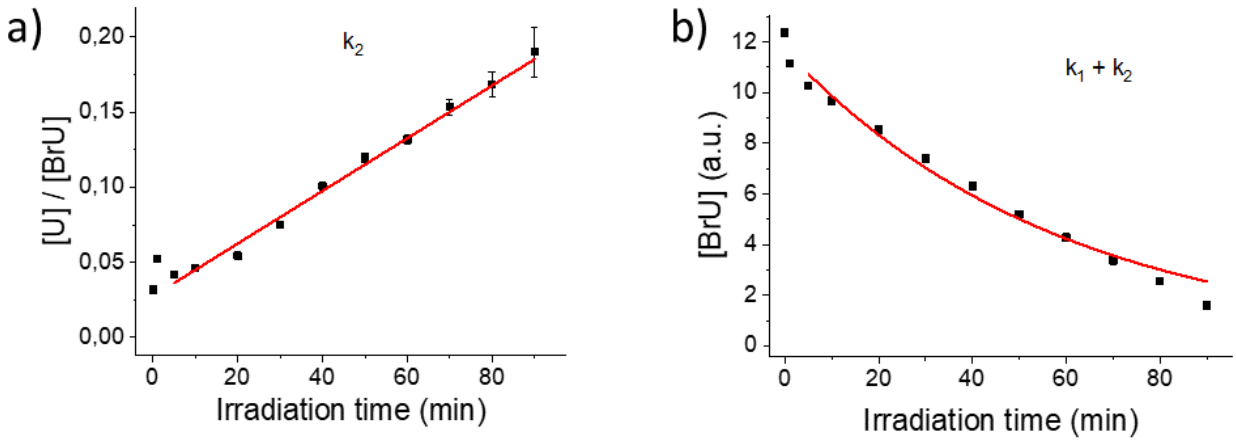

Figure 3: a) Ratio of the concentrations [U] and [BrU] plotted against the irradiation time t fit linearly to determine k_2 from the slope. b) Concentration [BrU] plotted as a function of the irradiation time t and fit with an exponential decay curve to determine k_1 and *k_2 form the decay constant.*

The reaction rates k_1 and k_2 have been determined at a fixed laser fluence for different repetition rates of the laser. The error bars of the reaction rates k_1 and $k_2$originate from the fit presented in Fig. 3 (see Figure 4). The reaction rate k_1 decreases significantly with higher laser repetition rates. At higher laser repetition rates, the time between two subsequent pulses is shorter. In consequence, there is less time following a laser pulse in which the BrU can adsorb on the cleaned surface before the AuNP is illuminated again. Therefore, the coverage of BrU on the AuNP surface during the pulse is lower at higher laser repetition rates, as the adsorption time for BrU is shortened. Lower concentrations of BrU on the AuNPs, i.e. in the areas of the highest temperatures, result in decreasing reaction rates for k_1. This trend is in accordance with results published previously.[25] Nevertheless, for k_2 no dependency on the repetition rate has been observed. k_2 represents the C-Br bond cleavage leaving the U ring intact. The C-Br bond of BrU is a predetermined breaking point of the molecule and can be efficiently cleaved by the dissociative attachment of low energy electrons, and also at elevated temperatures it is the first bond to break.[35] However, both processes might occur as well in the vicinity of the AuNP surface, and do not require an adsorption of the molecules. Furthermore, the conditions directly on the AuNP surface are extreme in terms of temperatures and pressures. Hence, it is unlikely that in adsorbed BrU molecules only the C-Br bond will be cleaved under laser irradiation prior desorption leaving the U ring intact.

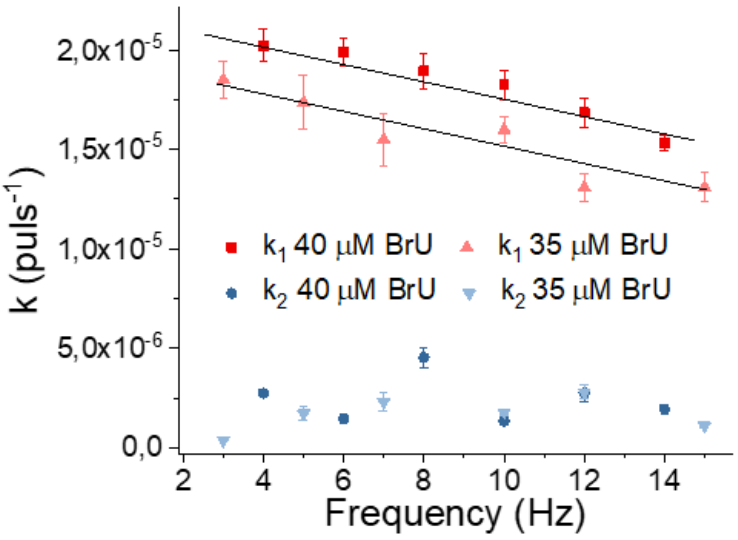

Figure 4: Reaction rates k1 (red) and k2 of BrU (blue) as a function of the laser repetition rate for two different initial concentrations of BrU (dark and light, respectively). Black lines are plotted to guide the eye.

Moreover, the reaction rates have been determined as a function of the maximum laser fluence (see Figure 5 a). For this purpose, the distance of the surface of the AuNP/BrU solution to the focus of the laser beam was varied using a mechanical stage. Due to this setup the photon fluence can be varied while keeping the power of the laser pulses constant. Even though the laser pulses have a Gaussian shape and the divergent laser beam widens during the passage through the AuNP/BrU solution leading to a spatially inhomogeneously distributed fluence, the maximum laser fluence is proportional to the average fluence in the solution. The reaction rates k_1 and k_2 show the same behavior as a function of the laser fluence, whereas k_1 is typically almost one order of magnitude higher than k_2. Up to a laser fluence of around 10^{13} W/m^2 the reaction rates are increasing with the laser fluence, however, for higher fluences (> 10^{13} W/m^2) the reaction rates are decreasing. A threshold, where k_2 is significantly increased with respect to k_1 due to an enhanced generation of thermionic electrons as predicted previously by Pyatenko et al. has not been observed.[20] In the predictions of the threshold nanoparticles of constant size have been assumed, nevertheless, the size of the generated nanoparticle fragments significantly depends on the laser fluences. The size of the nanoparticles influences strongly the absorption of the AuNPs at 532 nm due to the LSPR. In Figure 5 b) the absorbance at a wavelength of 532 nm has been plotted against the laser power, showing a decreasing absorbance with increasing laser fluence reaching a minimum at ~10^{13} W/m^2 as well. In general, small AuNPs exhibit LSPRs with lower intensities, which are centered at comparably lower wavelength. The decrease of the LSPRs as a function of the laser power is indicating a stronger fragmentation of the AuNPs at higher laser powers. Nevertheless, the resulting decreased absorption at 532 nm results in a lower energy absorption by the AuNP solution limiting the heating of the AuNPs and leading to stagnating or even reduction of the reaction rates at high fluences. At high laser fluences, especially for the irradiation of larger AuNPs, the ignition of plasmas has been observed.[29] Since, the plasmas occur statistically their role in the decomposition of the AuNPs and the molecules could not be evaluated.

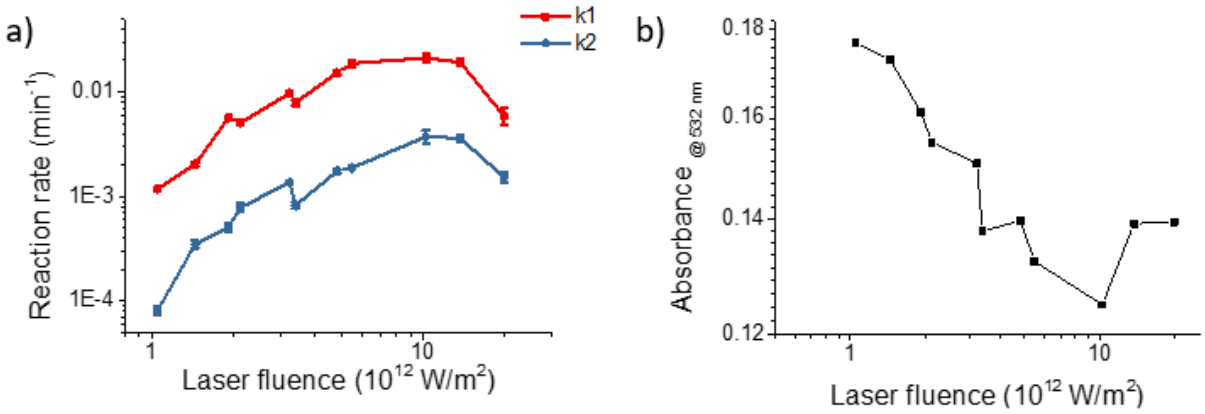

Figure 5: a) Reaction rates k1 and k2 plotted as a function of the laser fluence. b) Absorbance of AuNP/BrU solution at 532 nm after 20 minutes irradiation plotted against the laser fluence.

Although the LSPR absorption is decreasing with higher laser fluence, the reaction rates increase up to a maximum fluence of 10^{13} W/m^2. This might be explained by an increased surface area of the smaller AuNPs, since the number of gold atoms in the solution remains constant under the irradiation. However, also a possibly higher temperature around the AuNPs might be responsible for the higher reaction rates. In order to determine the surface area A_S of the AuNPs, the size distribution of the AuNPs after an irradiation for 20 minutes has been determined by AFM for six different laser fluences. In Figure 6 a) and b) typical AFM images of the AuNPs after the irradiation are shown. The diameter of the AuNPs has been determined from the height of the AuNPs and the normalized size distributions of the AuNPs are shown in Figure 6 c). For all studied laser fluences 500 -3000 AuNPs have been analyzed. In all cases the sizes of the AuNPs after the irradiation was reduced from 40 nm to below 10 nm. With the knowledge of the normalized size distribution of the AuNPs the overall surface area of the AuNPs in the solution can be calculated using the following equation:

$$A_S = \frac{V_{gold}}{\sum P(r) \cdot V(r)} \cdot 4\pi \cdot \sum P(r) \cdot r^2 \qquad (10)$$

V_{gold} is the total volume of the AuNPs in the solution, r is the radius of the AuNPs, $P(r)$ is the percentage of AuNPs with a radius r in the solution determined from the histograms shown in Fig 6 c) and SI 4 and $V(r)$ is the volume of an AuNP with a radius r. In Figure 6 d) the surface area is plotted as a function of the laser fluence revealing an increase of the surface area with the laser fluence. The presented error bars originate from the statistical error of the AuNP counting (see SI for details).

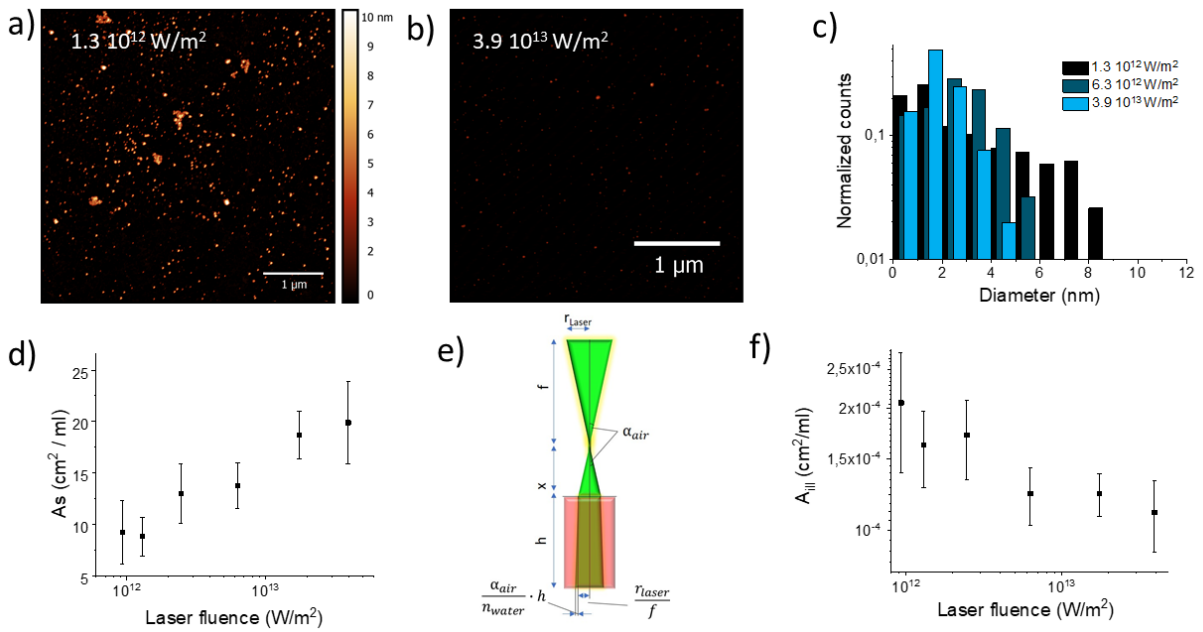

Figure 6: AFM image of AuNPs dried on a mica substrate illuminated for 20 min with a maximum laser fluence of a) 1.5 10^{12} W/m² and 4.3 10^{13} W/m² respectively. c) Normalized size distribution of AuNPs irradiated using different laser fluences. d) Surface area of the irradiated AuNPs determined using equation (12) as a function of the laser fluence. e) Sketch of the laser beam propagation after passing the focusing lens according to geometrical optics. f) Illuminated surface area during one laser pulse as a function of the laser fluence after irradiation for 20 min.

It needs to be considered that at higher laser fluences a smaller fraction of the solution is illuminated. In consequence, the illuminated surface area A_{ill} of the AuNPs needs to be determined to evaluate the effect of the surface area on the reaction rates. For this purpose, the illuminated volume V_{ill} for certain laser fluences has been calculated using basic geometrical optics assuming a simplified model of the laser beam path. The beam path in the solution has a truncated cone shape. A sketch of the beam propagation after the final focusing lens is presented in figure 6 e). The illuminated volume can be calculated by:

$$V_{ill} = \frac{\pi \cdot h}{3}\left[\left(\frac{x}{f}\cdot r_{Laser}\right)^2 + \left(\frac{x}{f}\cdot r_{Laser}\right)\left(\frac{r_{Laser}}{f\cdot n_{water}}\cdot h + \frac{x}{f}\cdot r_{Laser}\right) + \left(\frac{r_{Laser}}{f\cdot n_{water}}\cdot h + \frac{x}{f}\cdot r_{Laser}\right)^2\right] \qquad (11)$$

From the ratio of V_{ill} to the total volume of the solution V_{total} the illuminated area A_{ill} can be calculated by using equation (11):

$$A_{ill} = \frac{V_{ill}}{V_{total}}\cdot A_S \qquad (12)$$

In Figure 6 f) A_{ill} is plotted as a function of the laser fluence, revealing a decrease of A_{ill} with the fluence, although the relative error of the calculation is large. Hence, the increased reaction rates at higher laser fluences might not be solely explained by an increased surface area of the illuminated AuNPs.
Therefore, the absorbed heat Q_{abs} of an individual AuNP during a laser pulse has been calculated from the absorption cross section σ_{abs} of the irradiated AuNPs and the laser fluence I:

$$Q_{abs} = \sigma_{abs} \cdot I \qquad (13)$$

For small nanoparticles mainly the absorption is contributing to the extinction and the scattering can be neglected. Thus, the UV-Vis data presented in Fig. 5 b) has been used to estimate the absorption cross section σ_{abs} of the irradiated AuNP solution by using the Lambert Beer law.

$$Abs = l \cdot \sigma_{abs} \cdot N_{AuNP} \qquad (14)$$

The number of AuNPs per unit volume N_{AuNP} of the irradiated AuNP solution has been determined by:

$$N_{AuNP} = \frac{V_{AuNP\ 40nm}}{\sum P(r) \cdot V(r)} \cdot N_{AuNP\ 40nm} \qquad (15),$$

where $V_{AuNP\ 40nm}$ is the volume of an AuNP with a size of 40 nm and $N_{AuNP\ 40nm}$ is the initial number of 40 nm AuNPs per unit volume in the solution prior irradiation.

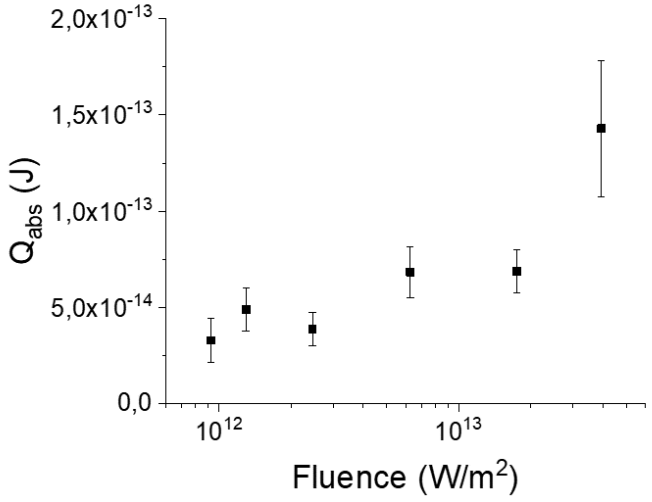

Figure 7: Heat absorbed by a single AuNP in one 16 mJ Laser pulse plotted as a function of the laser fluence.

In Fig 7 Q_{abs} is plotted as a function of the laser fluence revealing an increase of Q_{abs} with the laser fluence leading to a higher temperature of the individual AuNPs. Hence, the increase of the reaction rates with the laser fluence might be caused by an increased temperature around the AuNPs and possibly likewise by an increased generation of reactive species such as low energy electrons, even though the total absorption of light in the solution (see Fig. 5b) and the illuminated surface area (see Fig. 6 f)) are smaller. Nevertheless, the time between two laser pulses illuminating the same AuNP is longer for a smaller illuminated area and further the temperature gradient leads to a migration of molecules towards the AuNP surface[9], thus also the effect of adsorption on the decomposition rate cannot be neglected in this context.

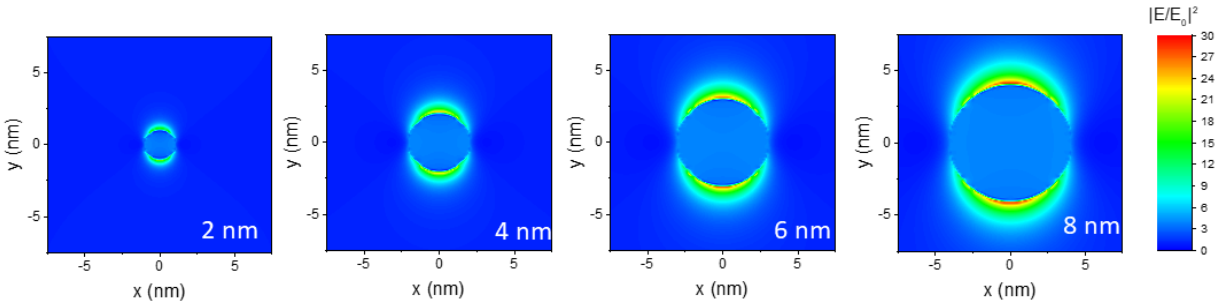

Figure 8: FDTD-calculation of the electrical field enhancement $|E/E_0|^2$ of AuNPs with a size of 2 nm, 4 nm, 6 nm and 8 nm respectively in an aqueous medium at a wavelength of 532 nm.

In order to evaluate the possible impact of multi-photon processes, the enhancement of the electrical field $|E/E_0|^2$ in the surrounding of the AuNPs has been determined by FDTD simulations. The simulations have been performed for spherical AuNPs with a size between 2 nm and 8 nm, which are typically generated under the described experimental conditions. In Figure 8 $|E/E_0|^2$ is plotted in the x-y plane crossing the center of the particle. For AuNPs a diameter of 2 nm the intensity enhancement is comparably small, not exceeding a factor of ~15 at the spots with the highest enhancement. Furthermore, the spots with a high enhancement are very localized close to the particle surface. In a distance of around 1 nm to the surface a significant enhancement of $|E/E_0|^2$ is no longer observable. With an increasing size of the AuNPs the intensity enhancement in the vicinity of the particles is increased. However, even for AuNPs with a diameter of 8 nm the maximum intensity enhancement is not exceeding a factor of 30. Irradiation of a BrU solution for several hours at high laser fluences in the absence of AuNPs did not lead to a change in the π-π* resonance (see SI 1). For U and Thymine a threshold multiphoton excitation leading to the fragmentation of the molecules have been observed at energies involving at least three 532 nm (2.33 eV) photons.[4,18] In consequence it is very unlikely to observe a significant contribution of multiphoton effects due to the laser irradiation in the present experiments, as the volumes with a comparably high enhancement are very localized and correlate with the volumes, where also the highest temperatures will occur, thus a thermal decay of possible photoproducts is likely.

Conclusion:

In summary, the kinetics of two decomposition pathways of BrU adsorbed on AuNPs induced by pulsed laser illumination have been tracked by UV-Vis spectroscopy and reaction rates have been determined by a kinetic model. The decomposition rates for the fragmentation of the BrU ring structure depend on the fluence, the repetition rate of the laser and the starting concentration of BrU. At higher laser fluences the AuNPs are decomposed and the surface area increased leading also to higher temperatures. However, on the other hand the irradiated volume is decreased and the plasmonic response is significantly lowered. Hence, these opposing effects are leading to a trade-off limiting the decomposition rates. The cleavage of the C-Br bond leaving the residual molecule intact is most likely independent of the adsorption of the molecules on the AuNPs. This process is probably electron or thermally induced, and multiphoton excitation processes are very unlikely. As the irradiation parameters are interlinked with the optical and thermal properties of the generated AuNP substrates, the tunability of the reaction kinetics of the system underlies restrictions regarding the accessible nanoscopic reaction conditions.

Acknowledgements

The authors acknowledge the financial support from Deutsche Forschungsgemeinschaft (Project No. 230710387) Fundação para a Ciência e a Tecnologia (FCT-MCTES), Radiation Biology and Biophysics Doctoral Training Programme (RaBBiT, PD/00193/2012); UID/Multi/04378/2019 (UCIBIO); UID/FIS/00068/2019 (CEFITEC); Associate Laboratory for Green Chemistry - LAQV which is financed by national funds from FCT/MCTES (UID/QUI/50006/2019), and scholarship Grant Nº PD/BD/106032/2015 to Telma Marques.

[1] N. S. Abadeer and C. J. Murphy, The Journal of Physical Chemistry C **120,** 4691 (2016).
[2] H. Abdoul-Carime, M. A. Huels, F. Brüning, E. Illenberger, and L. Sanche, The Journal of Chemical Physics **113,** 2517 (2000).
[3] M. Aioub and M. A. El-Sayed, Journal of the American Chemical Society **138,** 1258 (2016).
[4] B. Barc, M. Ryszka, J. Spurrell, M. Dampc, P. Limão-Vieira, R. Parajuli, N. J. Mason, and S. Eden, The Journal of Chemical Physics **139,** 244311 (2013).
[5] E. Boulais, R. Lachaine, A. Hatef, and M. Meunier, Journal of Photochemistry and Photobiology C: Photochemistry Reviews **17,** 26 (2013).
[6] S. J. Chadwick, D. Salah, P. M. Livesey, M. Brust, and M. Volk, The Journal of Physical Chemistry C **120,** 10647 (2016).
[7] E. Cortés, Advanced Optical Materials **5,** 1700191 (2017).
[8] D. B. DUNN and J. D. SMITH, The Biochemical journal **67,** 494 (1957).
[9] M. Enders, S. Mukai, T. Uwada, and S. Hashimoto, The Journal of Physical Chemistry C **120,** 6723 (2016).
[10] G. D. Fasman, *CRC Handbook of Biochemistry and Molecular Biology* (CRC Press2019).
[11] G. González-Rubio, A. Guerrero-Martínez, and L. M. Liz-Marzán, Accounts of chemical research **49,** 678 (2016).
[12] S. Hashimoto, T. Katayama, K. Setoura, M. Strasser, T. Uwada, and H. Miyasaka, Physical chemistry chemical physics : PCCP **18,** 4994 (2016).
[13] S. Hashimoto, D. Werner, and T. Uwada, Journal of Photochemistry and Photobiology C: Photochemistry Reviews **13,** 28 (2012).
[14] K. Haume, S. Rosa, S. Grellet, M. A. Śmiałek, K. T. Butterworth, A. V. Solov'yov, K. M. Prise, J. Golding, and N. J. Mason, Cancer nanotechnology **7,** 8 (2016).
[15] D. Lin, R. He, S. Li, Y. Xu, J. Wang, G. Wei, M. Ji, and X. Yang, ACS chemical neuroscience **7,** 1728 (2016).
[16] J. R. Mejía-Salazar and O. N. Oliveira, Chemical reviews **118,** 10617 (2018).
[17] K. Metwally, S. Mensah, and G. Baffou, The Journal of Physical Chemistry C **119,** 28586 (2015).
[18] R. Pandey, M. Ryszka, T. da Fonseca Cunha, M. Lalande, M. Dampc, P. Limão-Vieira, N. J. Mason, J. C. Poully, and S. Eden, Chemical Physics Letters **684,** 233 (2017).
[19] M. D. Prados, W. Seiferheld, H. M. Sandler, J. C. Buckner, T. Phillips, C. Schultz, R. Urtasun, R. Davis, P. Gutin, T. L. Cascino, H. S. Greenberg, and W. J. Curran, International journal of radiation oncology, biology, physics **58,** 1147 (2004).
[20] A. Pyatenko, M. Yamaguchi, and M. Suzuki, The Journal of Physical Chemistry C **113,** 9078 (2009).
[21] Z. Qin and J. C. Bischof, Chemical Society reviews **41,** 1191 (2012).

[22] J. Rak, L. Chomicz, J. Wiczk, K. Westphal, M. Zdrowowicz, P. Wityk, M. Żyndul, S. Makurat, and Ł. Golon, The journal of physical chemistry. B **119,** 8227 (2015).
[23] F. Sauvage, J. Schymkowitz, F. Rousseau, B. Z. Schmidt, K. Remaut, K. Braeckmans, and S. C. de Smedt, Nano Today, 100837 (2020).
[24] R. Schürmann and I. Bald, The Journal of Physical Chemistry C **120,** 3001 (2016).
[25] R. Schürmann and I. Bald, Physical chemistry chemical physics : PCCP **19,** 10796 (2017).
[26] R. Schürmann and I. Bald, Nanoscale **9,** 1951 (2017).
[27] R. Schürmann, K. Ebel, C. Nicolas, A. R. Milosavljević, and I. Bald, The journal of physical chemistry letters **10,** 3153 (2019).
[28] R. Schürmann, K. Tanzer, I. Dąbkowska, S. Denifl, and I. Bald, The journal of physical chemistry. B **121,** 5730 (2017).
[29] A. A. Serkov, P. G. Kuzmin, I. I. Rakov, and G. A. Shafeev, Quantum Electronics **46,** 713 (2016).
[30] M. Strasser, K. Setoura, U. Langbein, and S. Hashimoto, The Journal of Physical Chemistry C **118,** 25748 (2014).
[31] Y. Takeda, T. Kondow, and F. Mafuné, The journal of physical chemistry. B **110,** 2393 (2006).
[32] Y. Takeda, T. Kondow, and F. Mafuné, Physical chemistry chemical physics : PCCP **13,** 586 (2011).
[33] Y. Takeda, F. Mafuné, and T. Kondow, The Journal of Physical Chemistry C **113,** 5027 (2009).
[34] T. Tsuji, S. Sakaki, H. Fujiwara, H. Kikuchi, M. Tsuji, Y. Ishikawa, and N. Koshizaki, The Journal of Physical Chemistry C **122,** 21659 (2018).
[35] J. C. Tully, Science (New York, N.Y.) **312,** 1004 (2006).
[36] S. Wang, L. Fu, Y. Zhang, J. Wang, and Z. Zhang, The Journal of Physical Chemistry C **122,** 24421 (2018).
[37] K. A. Willets and R. P. van Duyne, Annual review of physical chemistry **58,** 267 (2007).
[38] K. Yamada, K. Miyajima, and F. Mafuné, The Journal of Physical Chemistry C **111,** 11246 (2007).
[39] M. Zdrowowicz, B. Michalska, A. Zylicz-Stachula, and J. Rak, The journal of physical chemistry. B **118,** 5009 (2014).
[40] D. Zhang, B. Gökce, and S. Barcikowski, Chemical reviews **117,** 3990 (2017).
[41] Y. Zhang, S. He, W. Guo, Y. Hu, J. Huang, J. R. Mulcahy, and W. D. Wei, Chemical reviews (2017).
[42] A. R. Ziefuß, S. Reichenberger, C. Rehbock, I. Chakraborty, M. Gharib, W. J. Parak, and S. Barcikowski, The Journal of Physical Chemistry C **122,** 22125 (2018).